Asian Journal of Chemistry; Vol. 37, No. 3 (2025), 529-537

ASIAN JOURNAL OF CHEMISTRY

https://doi.org/10.14233/ajchem.2025.33205

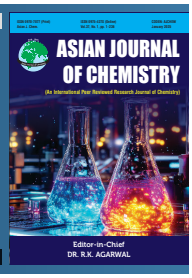

Development of High-Performance Composite from Sugarcane Bagasse and Multi-Walled Carbon Nanotubes for Enhanced Adsorption Applications

AMEL Y. AHMED[1,*] and IZZELDIN A.A. HAMZA[2]

[1]Department of Chemistry, Faculty of Science, King Faisal University, PO. Box 380, Al ahsa 31982, Saudi Arabia
[2]Department of Chemistry, Faculty of Science, University of Bahri, Khartoum 11111, Sudan

*Corresponding author: E-mail: aebrahim@kfu.edu.sa

Received: 15 December 2024; *Accepted*: 22 January 2025; *Published online*: 28 February 2025; AJC-21907

A novel composite of sugarcane bagasse with multi-walled carbon nanotubes (MWCNTs) in the ratio of 3:1 (m/m), respectively, was prepared. The bagasse was initially combined with functionalized MWCNTs using an HNO_3-H_2SO_4 mixture, after which it was crosslinked with glutaraldehyde. Several characterization techniques like SEM, TEM, FTIR, Raman spectroscopy and thermal gravimetric analysis, were used to demonstrate the successful functionalization of the MWCNTs and the covalent anchorage of the bagasse onto the functionalized MWCNTs. The composite was subsequently evaluated alongside bagasse for its effectiveness in removing heavy metal ions from a multi-component metal ion mixture through batch adsorption studies. The findings indicated the enhanced sorption properties for some heavy metals. This composite, therefore, shows good potential for applications that involve pre-concentration and removal of water pollutants.

Keywords: Sugarcane bagasse, Multi-walled carbon nanotubes, Composite adsorbent, Heavy metal ions, Green chemistry.

INTRODUCTION

Sugarcane bagasse is the fibrous residue leftover after the extraction of juice from sugarcane. In South Africa, the sugar industry crushes over 20 million tons of sugarcane and about 5 million tons of bagasse are produced annually. This agricultural residue is mainly composed of cellulose (42.3%), pentosans (25.1%), lignin (24.7%), ash (3.5%) and some nitrogen containing compounds [1]. These major biopolymer constituents have many hydroxyl and/or phenolic groups that can be chemically modified to form new materials with distinctive properties [2].

Due to its versatile properties, this biomass material has been used in many ways. For example, it is burnt for power generation at sugarcane mills and any excess energy is fed to national grids, processed into pulp for papermaking, used as a reactant in the chemical industry and for the production of animal feed, ethanol, enzymes and food additives. A report by Gurgel & Gil [3], among others [4-7], indicates that a large amount of bagasse is still not effectively reutilized [8,9]. Due to the large quantities of bagasse produced and the fact that it is an environmentally friendly and renewable resource, which would promote the green chemistry principles, there has been a growing interest towards the development and optimization of procedures that use this agro-industrial waste as a valuable raw material. One area of application is for the minimization or removal, of trace pollutants, such as heavy metals, in the environment [10].

Rapid industrialization has not made this challenge easy and instead has increased the concentrations of hazardous heavy metals in wastewaters. Since these metals are non-biodegradable and can be accumulated in living tissues and can thereby cause various diseases and disorders, they must be removed prior to effluent discharge. Adsorption has been shown to be a cost-effective and efficient means of heavy metal removal. Several studies [11,12] have shown that agricultural wastes with little or no economic value, that often cause a disposal problem, can be used as suitable adsorbents for environmental pollutants. The use of bagasse as an adsorbent material for the removal of metal ions and organic compounds from water and wastewaters already occurs [3,13-17]. Nevertheless, similar to several types of plant wastes, its ability to adsorb is limited and requires chemical enhancement. Hence, study into the inclusion of other materials such as carbon nanotubes (CNTs) has become increasingly important.

CNTs have aroused widespread attention because of their unique physicochemical properties which include electrical and thermal properties [18]. These advantageous properties include large surface areas [19] and the ability of CNTs to be functionalized by introducing oxygen groups on their surface which enhances the development of materials with improved properties [20-22]. Multi-walled carbon nanotubes (MWCNTs) have recently been reported to have better adsorption affinity than other commonly used adsorbents for the removal of heavy metal ions [23-29] and organic compounds [30-32] from aqueous solutions. Their high mechanical strength makes them suitable for the formation of composites [33].

Although research on the chemical alterations of sugarcane bagasse exists, there are no studies addressing the development of a composite of sugarcane bagasse and MWCNTs for the extraction of heavy metals from aqueous solutions. Thus, the objective of this study is to develop, characterize and evaluate a bagasse/MWCNT composite for the removal of heavy metal ions from aqueous solutions under ambient conditions. To improve interfacial adhesion and achieve uniform dispersion of MWCNTs within the bagasse matrix, the nanotubes were treated with acid oxidation to introduce oxygen containing functional groups on their surfaces.

EXPERIMENTAL

Sugarcane bagasse was provided by Mr SNWalford of the Sugar Milling Research Institute (SMRI) in Durban, South Africa. Ferrocene (Sigma-Aldrich, South Africa, 98% purity), toluene (BDH Chemicals Ltd., England, 99.5% pure AR), hydrochloric acid (chemically pure reagent, Promark Chemicals, C CImelman (Pty) Ltd., South Africa, 32% w/w), nitric acid (Sigma-Aldrich, South Africa, 69% pure), sulfuric acid (Saarchem, Merck, South Africa, 99-100% pure), NaOH pellets (Merck Chemicals (Pty) Ltd, South Africa), glutaraldehyde (Merck, South Africa, 25% aqueous solution), $NaHCO_3$ (SMM Instruments, South Africa, chemically pure reagent), Na_2CO_3 (Sigma-Aldrich, Germany, ≥ 99.5% purity), lead powder (Saarchem, Merck, South Africa, chemically pure), granulated cadmium (Thomas Baker Chemicals, Mumbai, India, 99.9% AR), copper powder (Johnson Matthey Chemicals Ltd.), granulated zinc (Sigma-Aldrich, South Africa, 99.8% purity), chromium powder (Sigma-Aldrich, South Africa, 99.55% purity) and nickel powder (Sigma-Aldrich, South Africa, < 150 μm, 99.9% trace metal basis) were used as received. The gas mixture of H_2 in Ar (10% H_2 in Ar (v/v) was obtained from Afrox, South Africa and was certified to be 10.1% (v/v) H_2.

Sugarcane bagasse preparation: Sugarcane bagasse was first dried under sunlight for 72 h. The fibres were then manually broken into small pieces and dried at 100 ºC in an oven for approximately 24 h. The dried broken fibres were further milled with the aid of an electrical grinder with a tungsten ball and sieved through a 215 μm sieve. The resulting fine powder was washed with distilled water under stirring at 60 ºC for 1 h, filtered and dried in a vacuum oven for 12 h at 80 ºC.

Preparation of MWCNTs: MWCNTs were prepared by the thermal chemical vapour deposition (CVD) method. The reactor design and setup has been previously described [34]. In a typical reaction, the metal catalyst (ferrocene, 0.125 wt.%) was dissolved in the carbon precursor (toluene, 10 mL) and the solution was injected into the system at a rate of 0.8 mL min^{-1}. The transformed gases were then carried by a reducing carrier gas mixture of H_2/Ar (10/90 v/v), at a flow rate of100 mL min^{-1}, into a horizontal quartz tube housed in a cylindrical furnace heated at 800 ºC, where gas pyrolysis led to the deposition of a MWCNT layer on the substrate. The system was left at the maximum temperature for 45 min, after which the furnace was switched off and allowed to cool. The gas (H_2/Ar) flow was left running until the system temperature fell below 250 ºC. Thereafter, the carrier gas was switched off and the system was left to cool to ambient temperature overnight. The nanotubes were then collected from the hot zone by scraping the walls of the quartz tube. This procedure yielded 1.20 g of crude MWCNTs.

Purification of MWCNTs: Impurities were chemically removed from the crude MWCNTs by dispersing HCl (20 mL of 6 mol dm^{-3} HCl) under stirring for 6 h at room temperature. The tubes were subsequently filtered and washed over vacuum with distilled water until Universal indicator paper showed the pH of the filtrate to be neutral. The procedure was then repeated with 20 mL of 6 mol dm^{-3} HNO_3. Thereafter, the MWCNTs were oven-dried at 100 ºC overnight, ground and calcined at 300 ºC for 30 min to remove any amorphous carbon.

Functionalization of MWCNTs: In a further step, oxidation of purified pristine MWCNTs was carried out by refluxing them in an acid solution consisting of a mixture of concentrated nitric acid and sulfuric acid in the ratio of 3:1 (v/v), respectively. The MWCNT-acid mixture (0.3 g MWCNTs in 20 mL acid solution in a round-bottomed flask) was refluxed for 5 h at room temperature. The mixture was then neutralized by adding 1.0 mol dm^{-3} NaOH solution. The resulting suspension was vacuum filtered and the black powder deposited on the filter was washed with distilled water until Universal indicator paper showed the pH of filtrate solution to be neutral. The MWCNTs were further washed with ethanol and acetone and eventually dried in an oven at 120 ºC for 12 h. The yield was found to be 95.3%. The functionalized MWCNTs were characterized and used in the subsequent experiments.

Preparation of sugarcane bagasse/MWCNT composite: An amount of 1.0 g of fine dry bagasse powder was sonicated for 2 h in 50 mL of deionized water at room temperature until the mixture was homogeneous. Separately, approximately 0.33 g of functionalized MWCNTs were dispersed in deionized water (20 mL) and sonicated for 2 h. Glutaraldehyde (2 mL) was added to the bagasse suspension to crosslink the bagasse fibres. The two suspensions were then mechanically mixed and the mixture was continued to be stirred for 2 h to increase the homogeneity. The resulting black product (bagasse/MWCNT composite) was filtered, washed with water and left to dry overnight in a vacuum oven at 80 ºC. It was subsequently ground to a fine powder and stored for characterization.

Characterization: A field emission gun scanning electron microscope (JEOL JSM 6100, Tokyo, Japan) was used to obtain three dimensional SEM topographical information, at an electron acceleration voltage of 10 to 15 kV with a magnification between

10 to 50 000 diameters for suitable image contrast and a resolution of 10 nm to 50 nm. A high resolution transmission electron microscope (JEOL JEM-1010, Tokyo, Japan) was used for TEM image visualization. The micrographs from TEM were taken at an acceleration voltage of 200 kV. Infrared spectra were obtained by using a Fourier transform infrared spectrometer (Perkin-Elmer Spectrum RX1) using KBr method in the wave number range of 4000 to 400 cm^{-1}. The crystallinity of the crude and functionalized MWCNTs was determined with a DeltaNu Advantage 532™ Raman spectrometer. The excitation source was a Nd:YAG solid state crystal and the NuSpec™ software was used to manipulate the scan durations, which typically ranged between 10 to 59 s. All the spectra were recorded at room temperature in the spectral range of 200 to 3400 cm^{-1}. The thermal analysis of sugarcane bagasse, crude and functionalized MWCNTs and the bagasse/MWCNT composite was conducted with a TA Instruments SDTQ 600 instrument. A mass of 2 mg of each sample was placed in an aluminium pan and heated at a heating rate of 10 ºC min^{-1}.

Surface area analysis: The specific surface areas of bagasse, MWCNTs and bagasse/MWCNT composite were determined by nitrogen adsorption/desorption experiments at liquid nitrogen temperature with a Micromeritics ASAP 2020surface area and porosity analyzer. The Brunauer-Emmett-Teller (BET) model was applied to calculate the surface area. Approximately 250 mg of ground and homogenized samples were degassed at 200 ºC in N_2 overnight and this was followed by the surface area determination at 77 K.

Determination of acidic surface functional groups: The acidic functional groups on the surface of the bagasse, functionalized MWCNTs and bagasse/MWCNT composite were determined by means of the Boehm titration method [35]. For the determination of the acidic sites, an amount of 0.2 g of each materials was mixed with 20 mL of each of three base solutions (0.1 mol dm^{-3} NaOH, 0.1 mol dm^{-3} $NaHCO_3$ and 0.05 mol dm^{-3} Na_2CO_3) in 100 mL plastic bottles with stoppers. The mixtures were shaken in a thermostated shaking water bath for 24 h at 28 ºC. The solutions were filtered through Whatman No. 1 filter paper and aliquots were titrated with 0.1 mol dm^{-3} HCl.

Batch adsorption: A multicomponent solution containing Cd(II), Cr(III), Cr(VI), Cu(II), Ni(II), Pb(II) and Zn(II) each at the same concentration of 20 mg dm^{-3} and pH 6.5 was used for adsorption studies. Batch adsorption experiments were performed by mixing 1.0 g of bagasse or bagasse/MWCNT composite with 50 mL of multi-metal ion solution in 100 mL plastic bottles with stoppers. The mixtures were agitated in a thermostated shaking water bath for 24 h at a constant speed of 150 rpm at 28 ºC and subsequently filtered through Whatman No. 1 filter paper. The filtrates were analyzed for the equilibrium concentrations of the unadsorbed metal ions by using inductively coupled plasma-optical emission spectrometry (Perkin-Elmer Optima 5300 DV spectrometer). The adsorption efficiency and adsorption capacity were calculated from eqns. 1 and 2, respectively:

$$\text{Adsorbed } (\%) = \left(\frac{C_i - C_{eq}}{C_i}\right) \times 100 \quad (1)$$

$$q_{eq} = \left(\frac{C_i - C_{eq}}{m}\right) \times V \quad (2)$$

where C_i is the initial concentration of metal ion (mg dm^{-3}), C_{eq} is the equilibrium concentration (mg dm^{-3}), m is the mass of adsorbent (g) and V is the volume of solution (mL).

RESULTS AND DISCUSSION

The crude MWCNTs obtained from the CVD synthesis contain impurities such as carbon spheres, carbon fibres and metal catalyst particles encapsulated in the closed tips and around the walls. In addition, sometimes unwanted amorphous carbon is obtained, which significantly affect the properties of the MWCNTs. Hence, a purification step was needed in order to remove the unwanted byproducts and metal particles and to open the closed MWCNT tips. After the purification step an oxidative functionalization step was performed on the MWCNTs. This step was essential in order to develop an adsorbent with good adsorption properties. As mentioned earlier, the adsorption capacity of bagasse is low and that of pristine MWCNTs is also low [36]. The introduction of oxygen-containing functional groups onto MWCNTs has been shown to improve their adsorptive capacities [37]. Functionalization of the MWCTs also served to make the CNTs more hydrophilic and easier to disperse in aqueous media and thereby combine with bagasse. The van der Waals interactions along the length of the CNTs naturally make them hydrophilic and if not functionalized they aggregate in aqueous solution. However, the purification and functionalization treatments of the MWCNTs introduce different defects on the hexagonal ring structure of the CNT walls and on the CNT tips. The closed tips open and some long tubes are shortened [22,27,38]. The effectiveness of the purification and functionalization steps was revealed when the various characterization methods were carried out.

Morphological studies: The microstructure of the crude, purified and functionalized MWCNTs was observed by means of SEM and high resolution TEM images. Significant differences in the morphology of MWCNTs before and after acid treatment were observed; the MWCNTs before acid treatment have smooth surfaces, are longer and some have closed tips as shown in Fig. 1a. In TEM micrograph (Fig. 1f), the metallic particles (arising from ferrocene catalyst) are distinctly observed in the form of black spots. As observed from the SEM image of purified MWCNTs (Fig. 1b), they are shorter in length, the tips have been partially opened and the metal particles have been removed from them. This is supported by the TEM results as shown in Fig. 1g, where it can further be observed that the purified MWCNTs are smooth and clean. Fig. 1c and h show a SEM and a TEM micrograph, respectively, of a functionalized MWCNT sample. It is clear that the tubes have curved and cylindrical shapes and that surface defects and agglomeration are enhanced after the acid treatment. The defects appear as grooves, which can be attributed to the functional groups introduced [39]. The functionalized MWCNTs appear shorter than the crude MWCNTs. Moreover, the outer diameters of the functionalized MWCNTs are larger than those of the crude MWCNTs, owing to the oxygen functional groups introduced after acid treat-

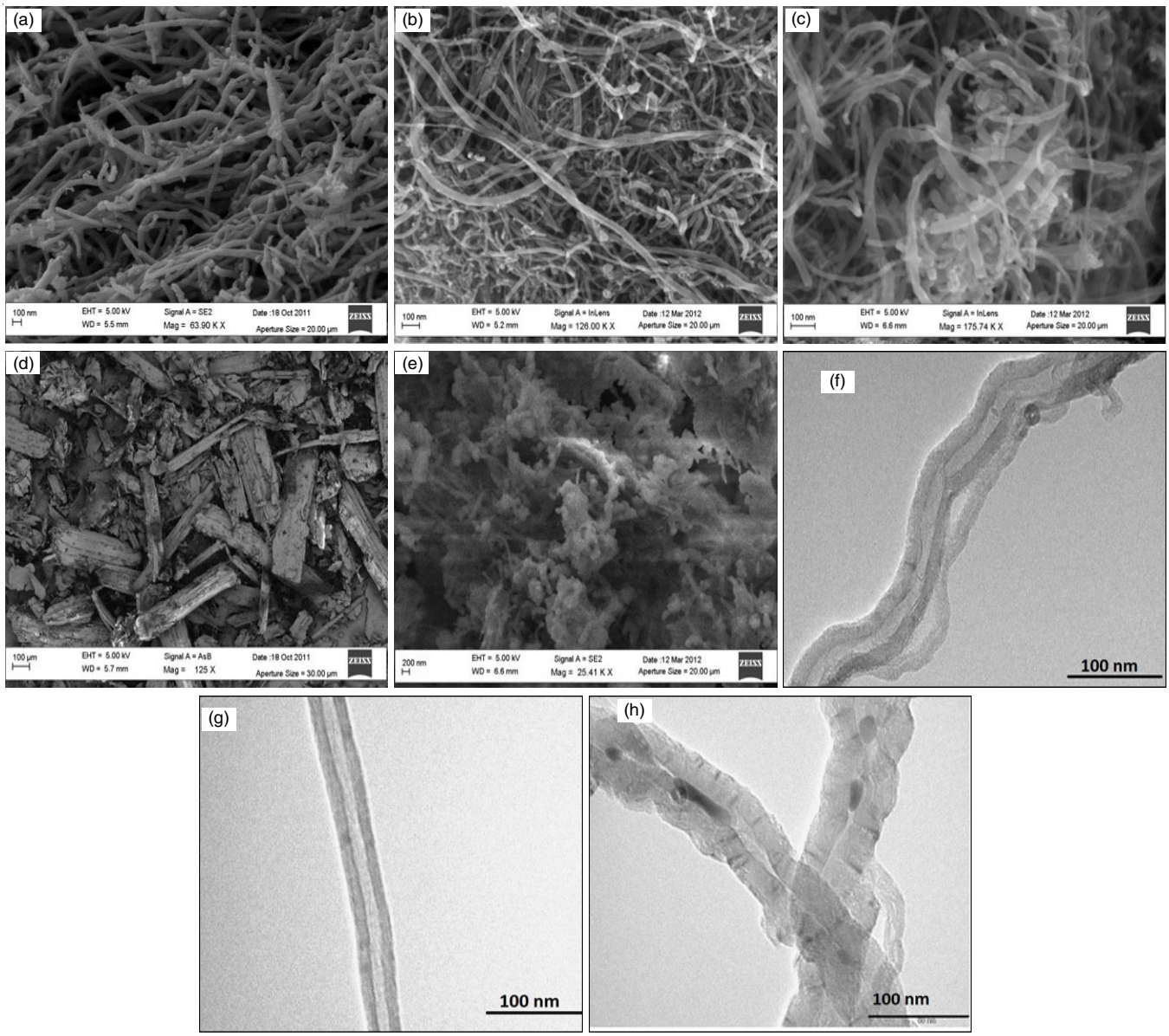

Fig. 1. SEM images of (a) crude MWCNTs, (b) purified MWCNTs, (c) functionalized MWCNTs, (d) bagasse and (e) bagasse/MWCNT composite and high resolution TEM images of (f) crude MWCNTs, (g) purified MWCNTs and (h) functionalized MWCNTs

ment, which also suggests that the functional groups have been successfully grafted on the surfaces of the MWCNTs. It is reported that oxidation, by a mixture of H_2SO_4 and HNO_3 acids, cuts the highly tangled long tubes into shorter, open-ended pipes and produces many functional groups on the sidewalls and at the open ends [40]. Further confirmation of the microstructure of the walls and surfaces of the functionalized MWCNTs was obtained by Raman spectroscopy.

The morphology and homogeneity of bagasse/MWCNT composite was visualized by means of SEM. Fig. 1 also shows SEM images of the surface of bagasse (Fig. 1d) and bagasse/MWCNT composite (Fig. 1e). The bagasse sample exists as fibres with no common structure. The image of bagasse/MWCNT composite shows that the components are homogeneously mixed and that the MWCNTs are embedded and well-dispersed within the bagasse material.

Functionalization: The FTIR spectra of bagasse, purified and functionalized MWCNTs and bagasse/MWCNT composite were recorded in order to confirm the presence of oxygen containing functional groups (Fig. 2). The main features of the spectrum of bagasse (Fig. 2a) are consistent with the presence of lignin, cellulose and hemicelluloses [41]. The strongest peaks occur at approximately 3328 and 1033 cm^{-1}. These arise from O-H and C-O stretching vibrations, respectively. The FTIR spectrum of pristine MWCNTs (Fig. 2b) is essentially featureless due to the poor infrared transmittance of these samples. However, two peaks are present in all the spectra (Fig. 2b-c) at approximately 3444 and 1636 cm^{-1}. These can be attributed to hydroxyl and carbonyl moieties, respectively and both absorptions increase on functionalization as expected. The presence of these peaks in the purified samples indicates that some degree of functionalization pre-exists. This is consistent with the

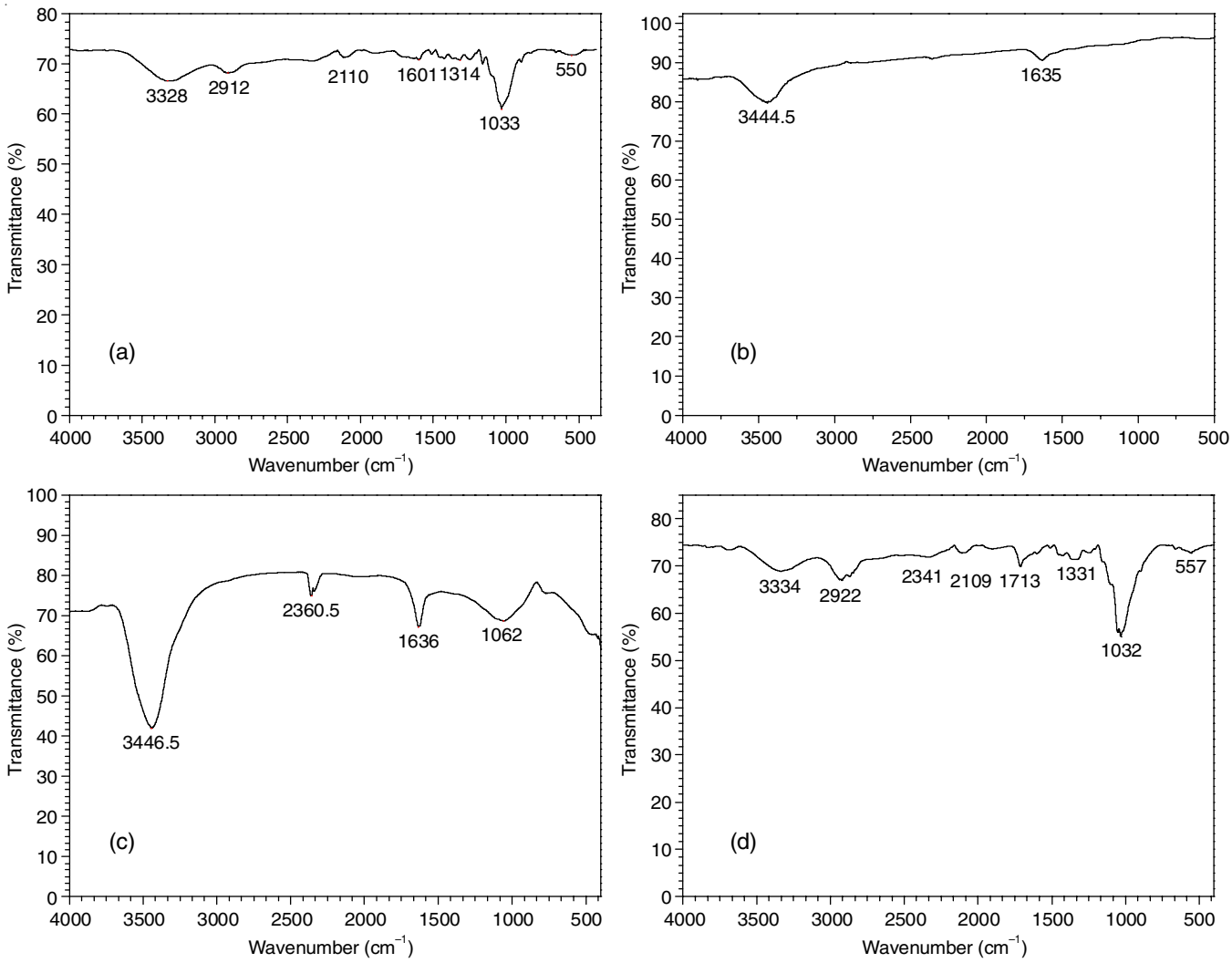

Fig. 2. FTIR spectra of (a) bagasse, (b) purified MWCNTs, (c) functionalized MWCNTs and (d) the bagasse/MWCNT composite

findings of Santagelo *et al.* [42], where a small degree of functionalization exists in pristine CNTs. There are differences in the spectra of the purified and functionalized MWCNTs which indicate that the structure of the CNTs has changed. The spectrum of the composite (Fig. 2d) shows a number of the peaks present in the spectrum of bagasse but a new peak emerges at 1713 cm^{-1} indicative of the C=O stretching mode and the covalent binding between the MWCNTs and bagasse. Hence, there is evidence that the MWCNTs were successfully functionalized and dispersed within the bagasse.

Crystallinity: Raman spectroscopy is a powerful physical technique that is widely used in the structural characterization of crude, purified and functionalized carbon nanotubes [43,44]. The technique shows a high sensitivity to the disorder structure on various carbon nanotube surfaces. It can be used to provide qualitative information about the status of the functionalization of MWCNT surfaces which corresponds to a functional group grafting on the surface of the MWCNTs. The Raman spectrum of crude MWCNTs showed the absence of the radial breathing modes expected in the range between 200-610 nm [14,45], which confirmed the MWCNT nature of the sample. The peak observed at 1344 cm^{-1} is attributed to the disorder structure of MWCNTs (D-band), such as defects of the graphite structure. The peak observed at 1595 cm^{-1} is attributed to the graphitic structure of MWCNTs (G-band). The ratio of the intensity of the defect band to the graphitic band is presented as the I_D/I_G parameter. The values of the I_D/I_G ratio (Table-1) can be used to estimate the relative extent of the MWCNT structural defects and hence to distinguish between the three different structural carbon nanotubes (crude, purified and functionalized). The intensity ratio (I_D/I_G) of the purified MWCNT sample was reduced from 0.99 to 0.96. It became more graphitic since the sample is more pure due to the removal of impurities (in particular, metal particles and amorphous carbons) from the surface. After functionalization of the MWCNTs, the relative intensity ratio (I_D/I_G) increased to 1.18 compared with that of the purified MWCNTs of 0.96. This shows that the introduction of the functional groups on the surface of the functionalized MWCNTs causes an increase in the D-band relative to the G-band and hence in the number of defects. Yudianti *et al.* [46] and Datsyuk *et al.* [38] report a (I_D/I_G) ratio of 1.68 and 1.01 respectively after the oxidation of MWCNTs by refluxing in a 1:3 (v/v) mixture of sulfuric and nitric acids as was done in this work.

TABLE-1
RAMAN DATA ON THE OXIDATIVE TREATMENT OF THE MWCNTs

MWCNT	Treatment	I_D/I_G[a]
Crude	–	0.99
Purified	6 M HCl, 6 M HNO_3	0.96
Functionalized	Conc. $HNO_3 + H_2SO_4$ (3:1 v/v)	1.18

[a]Ratio of the intensity of the defect band, I_D (arb. units) and the graphitic band, I_G (arb. units), as measured by Raman spectroscopy.

Thermal stability: Thermogravimetric analysis (TGA) was conducted to estimate the thermal stability of bagasse/MWCNT composite. The TG and DTG thermograms of samples of bagasse, MWCNTs and the bagasse/MWCNT composite obtained in air are presented in Fig. 3. The curves for bagasse show an initial mass loss below 100 ºC ascribed to the evaporation of physically adsorbed water. The DTG curve then shows two overlapping peaks with a maximum occurring at 320 ºC, which corresponds to the degradation of hemicellulose and cellulose. A second peak occurs with a maximum at 460 ºC due to the oxidation of char and non-volatile material [47]. The decomposition temperatures observed agreed well with those reported by Ramajo-Escalera *et al.* [48]. The amount of residue remaining at a temperature of 1000 ºC is approximately 6.5 wt.%. The TG and DTG curves of crude, purified and functionalized MWCNTs are presented in Fig. 3b-c, respectively. It is obvious that the weight loss starts at temperatures greater than 430 ºC. The weight loss below this temperature (3.5%) is due to the evaporation of absorbed moisture, combustion of organic impurities, or the evolution of the attached functional groups. For the crude MWCNTs, the maximum weight loss occurs at 650 ºC and corresponds to the combustion of CNTs [5,49]. Further heating of the MWCNTs up to 1000 ºC leaves a residue of approximately 16 wt.%, which is expected to be the residual catalytic iron metal particles from the synthesis. After purification an improvement of the thermal stability occurs and the maximum weight loss is reached at a higher temperature of 665 ºC. This is evidence of the successful removal of attached amorphous or structured carbon (*e.g.* carbon spheres) with acid treatment. This provides additional support for the findings derived from morphological analysis using SEM and TEM techniques. The residue remaining at a temperature of 1000 ºC decreased to 4.5 wt.% indicative of the successful removal of metal particles. After functionalization in a concentrated mixed acid solution, weight loss was observed in two steps. The first occurred at approximately 480 ºC and corresponds to the decomposition of the attached surface functional groups

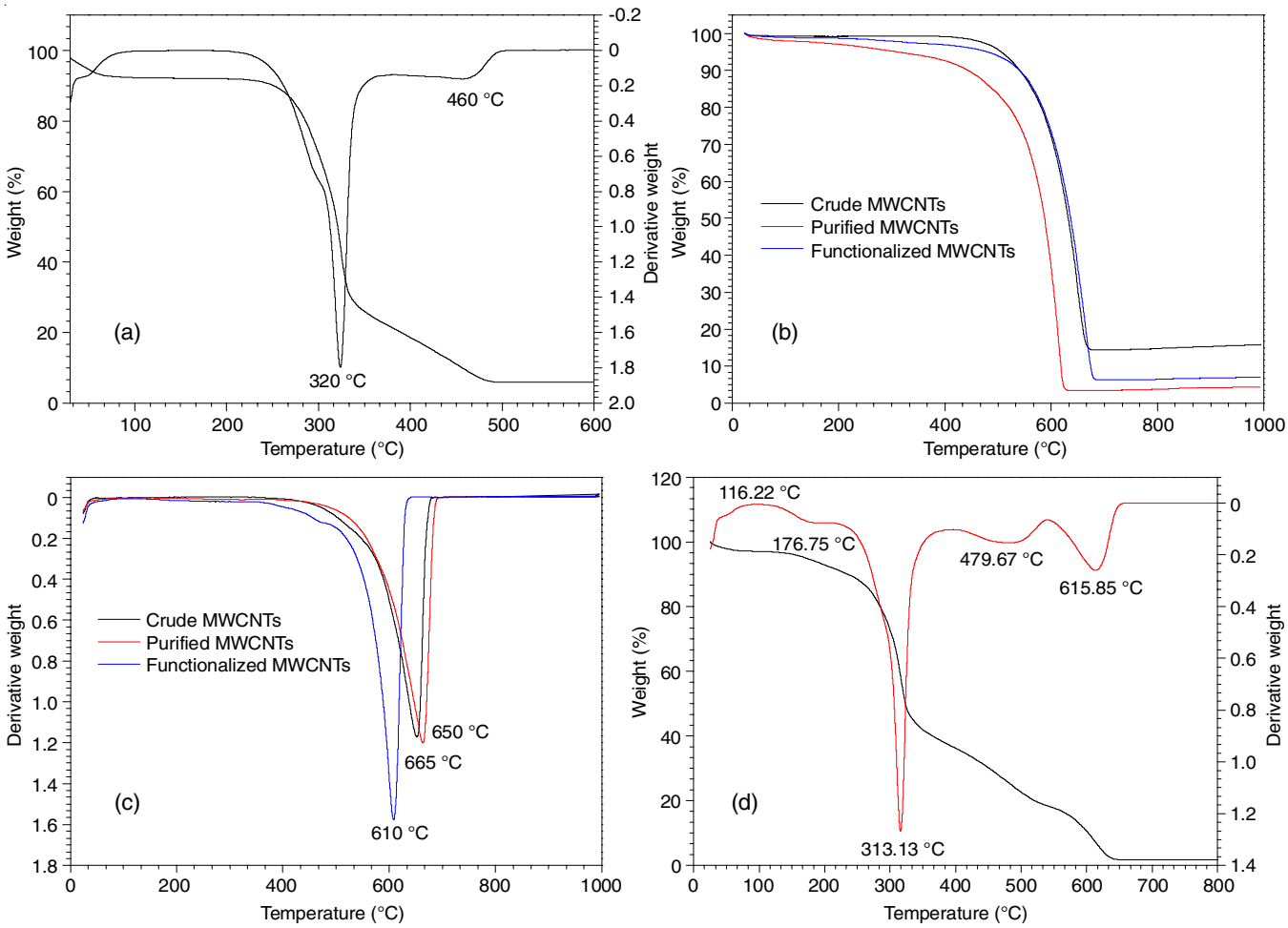

Fig. 3. (a) TG and DTG thermograms for bagasse, (b) TG thermograms for crude, purified and functionalized MWCNTs, (c) DTG thermograms for crude, purified and functionalized MWCNTs and (d) TG and DTG thermograms for the bagasse/MWCNT composite determined in an atmosphere of air with a flow rate of 50 cm^3 min^{-1} and a heating rate of 10 ºC min^{-1} from room temperature to 1000 ºC

and the release of CO_2.The maximum weight loss (90%) was reached in the second stage at 610 ºC, corresponding to the combustion of the CNTs. Further heating of the functionalized MWCNTs up to 1000 ºC left a residue of approximately 7.1 wt.%. These results are in full agreement with the reports of Scheibe *et al.* [50], Hsieh *et al.* [51] and Titus *et al.* [52].

The TG and DTG curves of the composite (Fig. 3d) show a number of weight losses occurring in distinct stages within the temperature range between 25-1000 ºC. Initially, between 50-115 ºC a weight loss of about 9.8 wt.% occurs which is ascribed to the evaporation of adsorbed moisture. Then four overlapping peaks occur with maxima at approximately 177, 313, 480 and 616 ºC. These losses arise from the components of bagasse, the functional groups on the MWCNTs and the decomposition of the MWCNTs. The thermal stability of the composite is intermediate between that of bagasse and the functionalized MWCNTs. The residue remaining at 1000 ºC is approximately 4 wt.% which is similar to the amount of residue remaining after the combustion of the MWCNTs.

Acidity of functional groups: The oxygen containing functional groups with acidic character on the surface of bagasse/MWCNT composite can be quantified by the Boehm titration method [35] and the results obtained are tabulated in Table-2. The carboxylic and hydroxyl functional groups are responsible for the acidic properties of the composite surface. The concentration of the strong acid groups on the composite surface was found from the $NaHCO_3$ titre. These are purported to be carboxylic groups and were found have a concentration of 0.9030 mmol g^{-1}. The total amount of strong and weak acidic functional groups on the composite was determined from the amount of Na_2CO_3 neutralized. The amount of the weak acid functional groups is the difference between these two titration values. For the composite this was 0.9810 mmol g^{-1} and this acidity arises from the laconic groups [53]. From the amount of NaOH neutralized, the total concentration of the phenolic, strong and weak acidic functional groups scan be determined (Table-2). The total amount of the acid functional groups on the composite surface is 3.5 mmol g^{-1}. It is observed that the total concentration of the acid groups on the composite surface is higher than for either the bagasse (1.7 mmol g^{-1}) or the functionalized MWCNTs (2.0 mmol g^{-1}) from which it is formed. The concentration of the phenolic functional groups was calculated from the difference between the three titration methods. For the composite the amount of phenolic groups was1.666 mmol g^{-1}. As reported by Santangelo *et al.* [42] in each case the concentration of the phenolic groups is greater than the sum of the other acidic groups. It is expected that these surface acid functional groups are suitable for metal ion removal from aqueous solutions. The results are in agreement with other studies in the literature [54-56].

Surface area analysis: The surface areas, pore volumes and pore diameters of the crude and functionalized MWCNTs, bagasse and bagasse/MWCNT composite were determined from nitrogen adsorption/desorption isotherms at liquid N_2 temperature (77 K). The specific surface area was calculated with the BET model. All the isotherms obtained could be classified as type IV isotherms according to the IUPAC1985 classification. The surface areas for the crude MWCNTs, functionalized MWCNTs, bagasse and bagasse/MWCNT composite are shown in Table-3. It is clear that crude MWCNTs possess a larger pore volume than the functionalized MWCNTs. This reduction in the pore volume of the MWCNTs after functionalization can be attributed to blockage of the pore cavity by the functional groups introduced. The surface areas of the crude MWCNTs and functionalized MWCNTs were found to be 124.8 and 177.6 $m^2 g^{-1}$, respectively. This indicates an increase in the functionalized MWCNT surface area. Bagasse shows a small surface area relative to the composite of bagasse and MWCNTs, which shows a larger surface area and thereby indicates the excellent dispersion of the MWCNTs within the bagasse fibres and, as a result, an improvement in nitrogen adsorption.

TABLE-3
SPECIFIC SURFACE AREA, PORE VOLUME AND AVERAGE PORE DIAMETER OF CRUDE MWCNTs, FUNCTIONALIZED MWCNTs, BAGASSE AND BAGASSE/MWCNTs COMPOSITE

Sorbent	Surface area ($m^2 g^{-1}$)	Pore volume ($cm^3 g^{-1}$)	Pore diameter (nm)
Crude MWCNTs	124.8	0.71	22.8
F-MWCNTs[a]	177.6	0.59	13.2
Bagasse	15.90	0.13	32.7
Composite	124.3	0.46	14.7

[a]F-MWCNTs: Functionalized multi-walled carbon nanotubes.

Application of bagasse/MWCNT composite for the adsorption of heavy metals: The effectiveness of the bagasse/

TABLE-2
CONCENTRATION OF ACIDIC GROUPS ON THE SURFACE OF BAGASSE, MWCNTs AND THE BAGASSE/MWCNT COMPOSITE DETERMINED BY THE BOEHM TITRATION METHOD

	Solution	$pH_{initial}$	$pH_{equilibrium}$	mmol g^{-1}	Functional group
Bagasse	NaOH	11.84	11.74	1.661	Phenolic, strong, weak acidic
	$NaHCO_3$	8.98	8.10	0.5427	Strong acidic
	Na_2CO_3	10.58	10.41	0.8734	Strong and weak acidic
F-MWCNTs[a]	NaOH	13.04	11.94	1.987	Phenolic, strong, weak acidic
	$NaHCO_3$	8.98	8.44	0.7564	Strong acidic
	Na_2CO_3	11.78	10.89	0.8729	Strong and weak acidic
Composite	NaOH	12.65	12.01	3.525	Phenolic, strong, weak acidic
	$NaHCO_3$	9.90	8.75	0.9030	Strong acidic
	Na_2CO_3	10.52	10.42	1.884	Strong and weak acidic

[a]F-MWCNTs: Functionalized multi-walled carbon nanotubes

MWCNT composite in adsorbing heavy metal ions, which contribute to environmental contamination in wastewater, was examined through analysis. These metals included copper, lead, cadmium, nickel, zinc and chromium ions since these metal ions are highly toxic in nature even at low concentrations. A batch adsorption procedure was conducted and the removal efficiency for each metal ion determined. It can be observed that the composite shows distinct improvement over bagasse for all the metal ions but particularly for Cu(II), Pb(II), Zn(II) and Cr(III) (Fig. 4). As with other studies involving the competitive adsorption of heavy metal ions with CNTs, the binding affinity of the composite is highest for Cu(II) and least for Ni(II) [57,58]. The superior metal adsorption ability of the composite can be attributed to the incorporation of the functionalized MWCNTs into bagasse. They markedly increased the surface area and the number of functional groups available for metal binding. In addition, the MWCNTs bring with them their strong binding ability as a result of electron delocalization over the hexagonal carbon rings on the surfaces. The dispersal of the MWCNTs between bagasse has also decreased the agglomeration between the CNTs and thereby exposed more sites for metal adsorption.

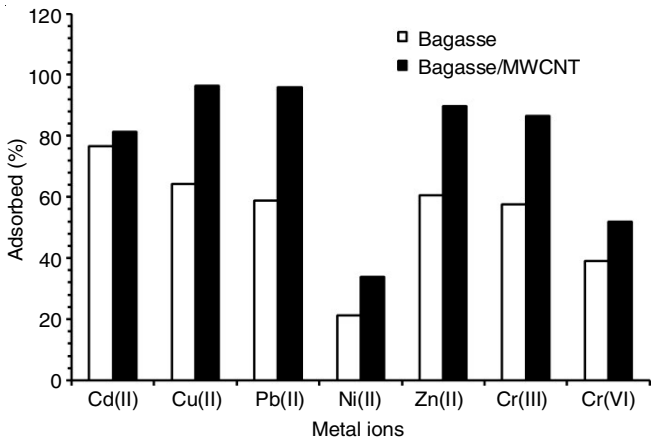

Fig. 4. Efficiency of heavy metal ion removal from aqueous solution by bagasse and the bagasse/MWCNT composite (50 mL of multicomponent metal ion solution in which each metal ion concentration is 20 mg dm^{-3}, 1.0 g of adsorbent, an agitation speed of 150 rpm, a contact time of 24 h and a temperature of 28 ºC)

Conclusion

A novel composite derived from sugarcane bagasse and functionalized MWCNTs has been successfully prepared. The morphological analysis of the composite confirms the homogenous distribution of the MWCNTs within the bagasse fibers. The incorporation of the functionalized MWCNTs in bagasse has improved both the thermal stability and surface area. The most significant change is in the number of acidic surface functional groups, which proved suitable for the removal of heavy metals from aqueous solutions. The adsorption capacity of the composite is much greater than that of bagasse. Therefore, this composite is an attractive and promising alternative for wastewater cleaning and environmental contamination control and supports the principles of green/sustainable chemistry.

CONFLICT OF INTEREST

The authors declare that there is no conflict of interests regarding the publication of this article.

REFERENCES

1. G.J.M. Rocha, V.M. Nascimento, A.R. Gonçalves, V.F.N. Silva and C. Martín, *Ind. Crops Prod.*, **64**, 52 (2015); https://doi.org/10.1016/j.indcrop.2014.11.003
2. L. Moghaddam, Z. Zhang, R.M. Wellard, J.P. Bartley, I.M. O'Hara and W.O.S. Doherty, *Biomass Bioenergy*, **70**, 498 (2014); https://doi.org/10.1016/j.biombioe.2014.07.030
3. L.V. Gurgel and L.F. Gil, *Water Res.*, **43**, 4479 (2009); https://doi.org/10.1016/j.watres.2009.07.017
4. Z. Aksu, *Process Biochem.*, **40**, 997 (2005); https://doi.org/10.1016/j.procbio.2004.04.008
5. Y. Jiang, H. Pang and B. Liao, *J. Hazard. Mater.*, **164**, 1 (2009); https://doi.org/10.1016/j.jhazmat.2008.07.107
6. P.L. Homagai, K.N. Ghimire and K. Inoue, *Sep. Sci. Technol.*, **46**, 330 (2010); https://doi.org/10.1080/01496395.2010.506903
7. I. Aloma, M.A. Martin Lara, I.L. Rodriguez, G. Blazquez and M. Calero, *J. Taiwan Inst. Chem. Eng.*, **43**, 275 (2012); https://doi.org/10.1016/j.jtice.2011.10.011
8. J.L.R.P. Filho, L.T. Sader, M.H.R.Z. Damianovic, E. Foresti and E.L. Silva, *Chem. Eng. J.*, **158**, 441 (2010); https://doi.org/10.1016/j.cej.2010.01.014
9. L.G.T. Carpio and F. Simone de Souza, *Renew. Energy*, **111**, 771 (2017); https://doi.org/10.1016/j.renene.2017.05.015
10. N.M. Noor, R. Othman, N.M. Mubarak and E.C. Abdullah, *J. Taiwan Inst. Chem. Eng.*, **78**, 168 (2017); https://doi.org/10.1016/j.jtice.2017.05.023
11. A. Mahvi, *Int. J. Environ. Sci. Technol.*, **5**, 275 (2008); https://doi.org/10.1007/BF03326022
12. S. Liu, H. Ge, C. Wang, Y. Zou and J. Liu, *Sci. Total Environ.*, **628-629**, 959 (2018); https://doi.org/10.1016/j.scitotenv.2018.02.134
13. B.A. Ezeonuegbu, D.A. Machido, C.M.Z. Whong, W.S. Japhet, A. Alexiou, S.T. Elazab, N. Qusty, C.A. Yaro and G. El-Saber Batiha, *Biotechnol. Rep.*, **30**, e00614 (2021); https://doi.org/10.1016/j.btre.2021.e00614
14. S. Islam, K.A. Shah, H. Mavi, A. Shaukla, S. Rath and Harsh, *Bull. Mater. Sci.*, **30**, 295 (2007); https://doi.org/10.1007/s12034-007-0049-y
15. O. Karnitz Jr., L.V.A. Gurgel, J.C.P. de Melo, V.R. Botaro, T.M.S. Melo, R.P. de Freitas Gil and L.F. Gil, *Bioresour. Technol.*, **98**, 1291 (2007); https://doi.org/10.1016/j.biortech.2006.05.013
16. V. Dos Santos, J. De Souza, C. Tarley, J. Caetano and D. Dragunski, *Water Air Soil Pollut.*, **216**, 351 (2011); https://doi.org/10.1007/s11270-010-0537-3
17. J. Mo, Q. Yang, N. Zhang, W. Zhang, Y. Zheng and Z. Zhang, *J. Environ. Manage.*, **227**, 395 (2018); https://doi.org/10.1016/j.jenvman.2018.08.069
18. M.S. Dresselhaus, G. Dresselhaus and P. Avouris, Carbon Nanotubes: Synthesis, Structure, Properties and Applications, Topics Applied Physics, Springer-Verlag, Berlin, Springer (2001).
19. A. Peigney, C. Laurent, E. Flahaut, R. Bacsa and A. Rousset, *Carbon*, **39**, 507 (2001); https://doi.org/10.1016/S0008-6223(00)00155-X
20. H. Yu, J.-G. Kim, D.-M. Lee, S. Lee, M.G. Han, J.-W. Park, S.M. Kim, N.D. Kim and H.S. Jeong, *Adv. Energy Mater.*, **14**, 2303003 (2024); https://doi.org/10.1002/aenm.202303003
21. H. Kuzmany, A. Kukovecz, F. Simon, M. Holzweber, C. Kramberger and T. Pichler, *Synth. Met.*, **141**, 113 (2004); https://doi.org/10.1016/j.synthmet.2003.08.018
22. K. Balasubramanian and M. Burghard, *Small*, **1**, 180 (2005); https://doi.org/10.1002/smll.200400118
23. M.I. Kandah and J.L. Meunier, *J. Hazard. Mater.*, **146**, 283 (2007); https://doi.org/10.1016/j.jhazmat.2006.12.019

24. D. Xu, X. Tan, C. Chen and X. Wang, *J. Hazard. Mater.*, **154**, 407 (2008); https://doi.org/10.1016/j.jhazmat.2007.10.059
25. S. Yang, J. Li, D. Shao, J. Hu and X. Wang, *J. Hazard. Mater.*, **166**, 109 (2009); https://doi.org/10.1016/j.jhazmat.2008.11.003
26. F. Fu and Q. Wang, *J. Environ. Manage.*, **92**, 407 (2011); https://doi.org/10.1016/j.jenvman.2010.11.011
27. M. Abdolkarimi-Mahabadi and M. Manteghian, *Fuller. Nanotub. Carbon Nanostruct.*, **23**, 860 (2015); https://doi.org/10.1080/1536383X.2015.1016608
28. A.H. Hammadi, A.M. Jasim, F.H. Abdulrazzak, A.M.A. Al-Sammarraie, Y. Cherifi, R. Boukherroub and F.H. Hussein, *Materials*, **13**, 2342 (2020); https://doi.org/10.3390/ma13102342
29. Y. Xu, A. Rosa, X. Liu and D. Su, *N. Carbon Mater.*, **26**, 57 (2011); https://doi.org/10.1016/S1872-5805(11)60066-8
30. B. Pan and B. Xing, *Environ. Sci. Technol.*, **42**, 9005 (2008); https://doi.org/10.1021/es801777n
31. K. Yang and B. Xing, *Chem. Rev.*, **110**, 5989 (2010); https://doi.org/10.1021/cr100059s
32. X. Ren, C. Chen, M. Nagatsu and X. Wang, *Chem. Eng. J.*, **170**, 395 (2011); https://doi.org/10.1016/j.cej.2010.08.045
33. L.M. Famá, V. Pettarin, S.N. Goyanes and C.R. Bernal, *Carbohydr. Polym.*, **83**, 1226 (2011); https://doi.org/10.1016/j.carbpol.2010.09.027
34. V.O. Nyamori, E.N. Nxumalo and N.J. Coville, *J. Organomet. Chem.*, **694**, 2222 (2009); https://doi.org/10.1016/j.jorganchem.2009.02.031
35. H.P. Boehm, *Carbon*, **40**, 145 (2002); https://doi.org/10.1016/S0008-6223(01)00165-8
36. S. Rosenzweig, G.A. Sorial, E. Sahle-Demessie and J. Mack, *Chemosphere*, **90**, 395 (2013); https://doi.org/10.1016/j.chemosphere.2012.07.034
37. E.J. Park, J.H. Jin, J.H. Kim, *et al.*, *Microchim. Acta*, **174**, 231 (2011); https://doi.org/10.1007/s00604-011-0605-4
38. V. Datsyuk, M. Kalyva, K. Papagelis, J. Parthenios, D. Tasis, A. Siokou, I. Kallitsis and C. Galiotis, *Carbon*, **46**, 833 (2008); https://doi.org/10.1016/j.carbon.2008.02.012
39. B. Nora, F. Fatirah, A. Zaiton and S. Shafinaz, *Dig. J. Nanomater. Biostruct.*, **7**, 33 (2012).
40. H. Modekwe and I. Ramatsa, *Environ. Res. Technol.*, **7**, 108 (2024); https://doi.org/10.35208/ert.1306840
41. K. Bilba and A. Ouensanga, *J. Anal. Appl. Pyrolysis*, **38**, 61 (1996); https://doi.org/10.1016/S0165-2370(96)00952-7
42. S. Santangelo, G. Messina, G. Faggio, S.H. Abdul Rahim and C. Milone, *J. Raman Spectrosc.*, **43**, 1432 (2012); https://doi.org/10.1002/jrs.4097
43. Y.P. Sun, K. Fu, Y. Lin and W. Huang, *Acc. Chem. Res.*, **35**, 1096 (2002); https://doi.org/10.1021/ar010160v
44. C. Vix-Guterl, M. Couzi, J. Dentzer, M. Trinquecoste and P. Delhaes, *J. Phys. Chem. B*, **108**, 19361 (2004); https://doi.org/10.1021/jp047237s
45. P. Rai, D.R. Mohapatra, K. Hazra, D. Misra, J. Ghatak and P. Satyam, *Chem. Phys. Lett.*, **455**, 83 (2008); https://doi.org/10.1016/j.cplett.2008.02.057
46. R. Yudianti, O. Holia and S. Sudirman, *Open Mater. Sci. J.*, **5**, 242 (2011); https://doi.org/10.2174/1874088X01105010242
47. G.J. Griffin, *Bioresour. Technol.*, **102**, 8199 (2011); https://doi.org/10.1016/j.biortech.2011.05.051
48. B. Ramajo-Escalera, A. Espina, J.R. García, J.H. Sosa-Arnao and S.A. Nebra, *Thermochim. Acta*, **448**, 111 (2006); https://doi.org/10.1016/j.tca.2006.07.001
49. L.S.K. Pang, J.D. Saxby and S.P. Chatfield, *J. Phys. Chem.*, **97**, 6941 (1993); https://doi.org/10.1021/j100129a001
50. B. Scheibe, E. Borowiak-Palen and R.J. Kalenczuk, *Mater. Charact.*, **61**, 185 (2010); https://doi.org/10.1016/j.matchar.2009.11.008
51. Y.C. Hsieh, Y.C. Chou, C.P. Lin, T.F. Hsieh and C.M. Shu, *Aerosol Air Qual. Res.*, **10**, 212 (2010); https://doi.org/10.4209/aaqr.2009.08.0053
52. E. Titus, N. Ali, G. Cabral, J. Gracio, P.R. Babu and M.J. Jackson, *J. Mater. Eng. Perform.*, **15**, 182 (2006); https://doi.org/10.1361/105994906X95841
53. B. Petrova, T. Budinova, B. Tsyntsarski, V. Kochkodan, Z. Shkavro and N. Petrov, *Chem. Eng. J.*, **165**, 258 (2010); https://doi.org/10.1016/j.cej.2010.09.026
54. Z. Wang, M.D. Shirley, S.T. Meikle, R.L.D. Whitby and S.V. Mikhalovsky, *Carbon*, **47**, 73 (2009); https://doi.org/10.1016/j.carbon.2008.09.038
55. H. Liu, F. Yang, Y. Zheng, J. Kang, J. Qu and J.P. Chen, *Water Res.*, **45**, 145 (2011); https://doi.org/10.1016/j.watres.2010.08.017
56. M. López-Mesas, E.R. Navarrete, F. Carrillo and C. Palet, *Chem. Eng. J.*, **174**, 9 (2011); https://doi.org/10.1016/j.cej.2011.07.026
57. Z. Gao, T.J. Bandosz, Z. Zhao, M. Han and J. Qiu, *J. Hazard. Mater.*, **167**, 357 (2009); https://doi.org/10.1016/j.jhazmat.2009.01.050
58. Y.B. Onundi, A.A. Mamun, M.F.A. Khatib, M.A.A. Saadi and A.M. Suleyman, *Int. J. Environ. Sci. Technol.*, **8**, 799 (2011); https://doi.org/10.1007/BF03326263